Title

Effective adsorption and visible light driven enhanced photocatalytic degradation of rhodamine B using ZnO nanoparticles immobilized on graphene oxide nanosheets

Journal

Results in Physics, 58

ISSN

2211-3797

Authors

Sayem, Abdulla

Suvo, Amran Hossen

Syed, Ishtiaque M

et al.

Publication Date

2024-03-01

DOI

10.1016/j.rinp.2024.107471

Results in Physics 58 (2024) 107471

Contents lists available at ScienceDirect

Results in Physics

journal homepage: www.elsevier.com/locate/rinp

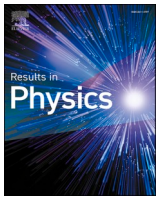

Effective adsorption and visible light driven enhanced photocatalytic degradation of rhodamine B using ZnO nanoparticles immobilized on graphene oxide nanosheets

Md. Abdulla Sayem [a,b], Md Amran Hossen Suvo [a,b], Ishtiaque M. Syed [a,c], Mahabub Alam Bhuiyan [a,b,*]

[a] Department of Physics, University of Dhaka, Dhaka 1000, Bangladesh
[b] Semiconductor Technology Research Centre, University of Dhaka, Dhaka 1000, Bangladesh
[c] Centre for Advanced Research in Sciences, University of Dhaka, Dhaka 1000, Bangladesh

ARTICLE INFO

Keywords:
GO-ZnO nanocatalysts
Adsorption
Visible light
Photo-degradation
rhodamine B dye

ABSTRACT

In this study, graphene oxide (GO), ZnO nanoparticles (NPs) and GO based ZnO nanocomposites (GO-ZnO) have been successfully synthesized by modified Hummer's method, chemical co-precipitation method and ultrasonication method, respectively. Powder X-ray diffraction (PXRD), transmission electron microscopy (TEM) and Fourier transform infrared (FTIR) spectroscopy were employed to study the crystallographic structure, phase, surface micro-morphology and different functional groups in the prepared catalysts. The optical band gap of pristine ZnO NPs was found in the UV region (3.2 eV), whereas the ZnO NPs immobilized on GO nanosheets possesses it in the visible wavelength region (2.67 eV). GO-ZnO catalysts demonstrate excellent degradation efficiency (97.7 %) within just 85 min due to its effective adsorption and visible light driven photocatalytic activity in the degradation of rhodamine B (RhB) dye. The adsorption capacity of GO-ZnO catalysts was found ~ 24 times higher with the second order kinetic rate constant as low as 0.0014 min • g/mg and the visible light driven photocatalytic activity was ~ 9 times faster when compared to unmodified ZnO catalyst. Effect of GO-ZnO catalyst dosages in the degradation of RhB was also conducted. The scavenger test firmly evidenced that super oxide radicals ($\bullet O_2^-$) play the lead role in RhB dye degradation process by GO-ZnO nanocomposites. Reusability studies of GO-ZnO catalysts demonstrate more than 91 % degradation efficiency up to 4 back-to-back cycles along with retaining the crystal structure. These findings suggest the viable application of GO-ZnO catalysts for the degradation of RhB dye in wastewater.

Introduction

Recent development of the world economy is firmly based on industrialization such as textile, tannery, food, pharmaceuticals, *etc.* However, they are producing/discharging many hazardous chemical compounds [1,2]. For instance, roughly one million tons of artificial dyes are produced worldwide and around 20 % of the worldwide total manufacturing of dyes is lost and discharged into textile effluents during the dying process [3,4]. These organic effluents are toxic, and persistent in nature due to their non-biodegradability, which cause not only environmental pollution but also life threatening for aquatic and human bodies [5,6]. These have garnered attention to scientific community as well as regulatory bodies [7]. An example of such hazardous organic dye is rhodamine B (RhB), which is extensively used in various industries *e.g.* textile, leather, printing and plastic industries [8]. Its chemical structure ($C_{28}H_{31}ClN_2O_3$, aromatic rings present in it) is such that the complex rings are non-biodegradable and exists in nature forever without any significant degradation and can cause serious threats to biological and human health [9]. Due to these burgeoning issues, it has become one of the focal points of research interest to many researchers and a numerous extensive research efforts have been directed towards the development of efficient and eco-friendly approaches for the removal and degradation of RhB dye from aqueous environments [10]. Several traditional strategies have been adopted to treat the discharged unwanted organic effluents in waste water, which includes bio-degradation, coagulation, filtration through membranes, ion exchange and flocculation [11].

* Corresponding author at: Department of Physics, University of Dhaka, Dhaka 1000, Bangladesh.
E-mail address: mahabub@du.ac.bd (M.A. Bhuiyan).

https://doi.org/10.1016/j.rinp.2024.107471
Received 7 December 2023; Received in revised form 30 January 2024; Accepted 10 February 2024
Available online 12 February 2024

However, these traditional methods are either expensive or requires further treatment, which has made them inefficient in waste water treatment [12,13].

The development of advanced oxidation process (AOP) such as photocatalysis has brought some hopes and currently gaining much attention in the waste water treatment due to its low cost and environment friendliness [11]. This photocatalytic degradation process involves the use of semiconducting nanomaterials to generate reactive species upon exposure to UV or visible light, which can subsequently degrade the complex organic effluents through the oxidative reaction mechanism [14,15]. Various semiconducting nanomaterials such as TiO_2, ZnO, WO_3, V_2O_5, MO_3, CdS, $BiVO_4$, *etc.* have been reported as photocatalysts so far [16–22]. Among those, an excessive care has been rewarded to ZnO due to its availability, low cost to prepare, chemical stability, biocompatibility, strong oxidizing capability and harmless makeup [23,24]. However, its wide optical band gap (3.22 eV) is not suitable for the electron-hole generation by visible light illumination, which hinders to use ZnO as a visible light driven photocatalyst [25]. Another issue of ZnO is the faster electron-hole recombination, which makes it an inefficient photocatalyst [26]. To overcome these major issues, numerous techniques have been employed such as metal, non-metal doping [27], forming heterojunctions [28], mixed phase structures [29], *etc.* All of these techniques were mainly focused on the increase of visible light absorption and creating charge separation. Recently, researchers have identified that some inexpensive adsorbent materials such as carbon nanotubes, graphene, graphene oxide, *etc.* can be employed to serve these purposes and thereby the adsorption and photocataysis have come to light as promising schemes for the degradation of organic pollutants [30]. Among the explored adsorbent materials, graphene oxide (GO), which has anionic 2D hexagonal structure of sp^2 hybridized carbon atoms with several oxygen based functional groups attached to it is comparatively easy to synthesis but demonstrates excellent adsorption property due to some noteworthy characteristics *e.g.* large surface area ($\sim$2600 m^2/g), hydrophilicity, high conductivity and transportation of electrons, and mechanical stability [31–35]. It is studied that mixing GO with metal oxide can enhance the adsorptivity of organic molecules on catalysts surface due to the $\pi-\pi$ conjugation structure, can act as an excellent acceptor for photogenerated electrons which can hinders the recombination process of photogenerated electron-hole pairs, thus can increase the oxidation rate, which in turn boost up the photocatalytic performance [36–38]. Furthermore, the presence of GO with metal oxide can cause a red shift towards the visible wavelength region with stronger absorbance of visible light due to the hybridization of oxygen functionalities of GO with metal oxides [39]. This makes GO based metal oxide semiconductors as visible light driven photocatalysts. Therefore, it is presumable that the synergistic effect in GO-ZnO nanocomposites has the ability to boost up the overall degradation efficiency of this GO-ZnO catalyst due to the effective adsorption and photocatalysis with compared to pristine ZnO catalyst and can be a viable candidate for the removal of effluents from waste water. Recently, several methods have been explored to prepare GO-ZnO nanocomposites, however, those techniques require severe synthesis conditions such as high pressure and temperature but provide low yield in terms of expense [40–45]. Furthermore, the reported literature illustrate that GO-ZnO catalysts were mostly utilized either for the removal of heavy metals such as Pb [46], Cr [47] and As [48], or for the photocatalytic degradation of methylene blue (MB) [43,45,49,50] and a few literature reported its application for the removal of other pollutants such as acetamiprid [51], brilliant green [52]. However, as per the available literature, the effectiveness of ZnO NPs immobilized on graphene oxide (GO) nanosheets has never been explored thoroughly for both the effective adsorption and visible light driven enhanced photocatalytic degradation of RhB. Considering the concern of environmental and health issues due to the presence of RhB in waste water and the potential effectiveness of GO-ZnO nanocomposites, a detail thorough study of this nanocatalyst for the degradation of life threatening RhB dye may help to realize its feasible application in RhB removal from waste water.

Therefore, this research aims to prepare ZnO nanoparticles immobilized on GO nanosheets (GO-ZnO nanocomposites) by a straight forward, facile, cost-effective method with high yield and to explore the combination of adsorption and visible light driven photocatalysis for the comprehensive and effective degradation of rhodamine B (RhB) dye from waste water. The corresponding kinetics has been studied in details. Thereafter, the effect of GO-ZnO catalyst dosages, role of radical species and cyclic ability has been investigated in thoroughly and finally a plausible degradation mechanism of RhB by using this GO-ZnO catalyst has been proposed with appropriate justification.

Experimental details

Chemicals and reagents

Sodium hydroxide pellets (NaOH) (98 % pure), sodium nitrate ($NaNO_3$) (99.5 % pure) used in our experiment were purchased from Loba Chemie Pvt. Ltd. Zinc acetate dehydrate ($Zn(O_2CCH_3)_2.(H_2O)_2$) (extra pure), Rhodamine B dye were purchased from Sisco Research Laboratories Pvt. Ltd. Sulfuric acid (H_2SO_4) (98 % pure), ethanol (extra pure) were purchased from Merck KGaA 25,064,293 Darmstadt. Sigma-Aldrich supplied graphite powder (extra pure) and potassium permanganate ($KMnO_4$) (extra pure). These chemical reagents used in this work were utilized straight out of the package without being further purification. In various stages, de-ionized (DI) water was used to prepare certain solutions and for washing purposes.

Synthesis of samples

Synthesis of graphene oxide (GO)

Graphene oxide (GO) was synthesized by the popular improved Hummer's method [53]. In brief, 2.5 g $NaNO_3$ was added in a 1000 mL conical flask containing 120 mL H_2SO_4. Next, 4.5 g of graphite powder was slowly added into the mixture. This mixture was stirred for 20 min at 20 °C and thereafter, it was cooled down to 0 °C by using an ice bath and 15 g $KMnO_4$ was added to it. This mixture was stirred at 0 °C for next 60 min and 250 mL DI water was added into the solution under continuous stirring. After some time, 20 mL of 30 % H_2O_2 was added dropwise to the mixture solution and the temperature was then increased to room temperature and continued the stirring for next 2 h at this temperature. Then the final solution was centrifuged at 6000 rpm for 10 min to collect the precipitate which was then washed with DI water and 10 % HCl for few times, and again twice with DI water. Finally, the washed precipitate sample was dried at 60 °C for 70 h in an oven and collected as graphene oxide (GO).

Preparation of zinc oxide (ZnO) nanoparticles

Using chemical co-precipitation method, ZnO nanoparticles was synthesized. Initially, 10 g of zinc acetate dehydrate was dissolved in 250 mL DI water at 25 °C. Then a 3 M NaOH solution was added sequentially to it under magnetic stirring. The addition of NaOH was stopped when the pH of the reaction becomes 12 but the stirring was continued for succeeding 30 min to achieve a homogenous mixture and thereafter left it for an hour to obtain precipitate, which was then rinsed several times with DI water and ethanol to clean the unreacted chemicals, followed by air drying for 12 h at 50 °C to evaporate the residuals. The baked sample was calcined for 4 h in a muffle furnace at 400 °C and crushed into powder by mortar-pestle system to obtain ZnO nanoparticles.

Synthesis of GO-ZnO nanocomposites

Synthesized ZnO nanoparticles were immobilized on GO nanosheets by a quite straightforward ultrasonication process. In a typical preparation process, firstly, 0.08 g GO was ultrasonicated in DI water for 30 min into which 0.24 g ZnO was added to it slowly. To obtain

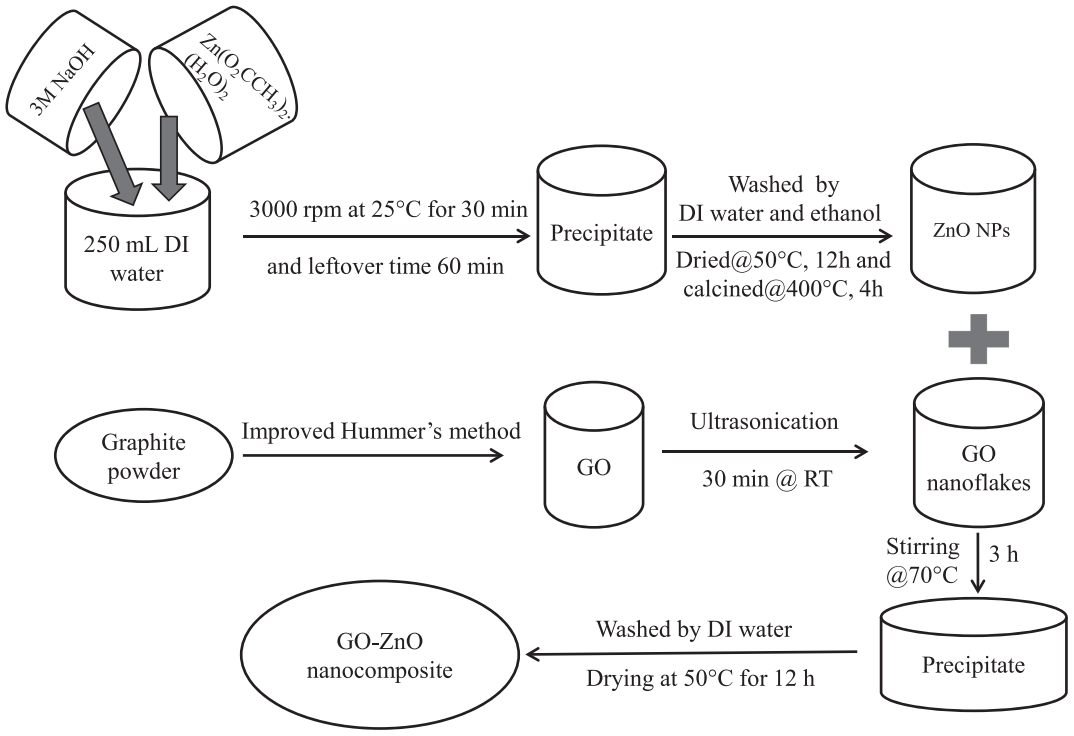

Scheme 1. Synthesis flow diagram to illustrate the different steps involved in the preparation of GO, ZnO NPs and GO-ZnO nanocomposites.

homogeneous dispersion solution, the mixture was stirred for 3 h at 70 °C. The precipitate was collected by centrifugation when the temperature come down to room temperature, followed by few times washing with DI water and air oven drying at 50 °C for 12 h. The acquired ZnO NPs immobilized on GO nanoleaves was labelled as GO-ZnO throughout the work. A complete flow diagram for the synthesis of GO-ZnO nanocomposites is depicted in Scheme 1.

Characterization of samples

Several techniques were employed and various measurements were carried out to investigate the successful synthesis of our prepared samples. In particular, an X-ray diffractometer from Rigaku Ultima IV company having *CuK-α* wavelength of 1.54056 Å was used to carry out all the powder XRD measurements. Fourier transform infra-red (FTIR) spectra were recorded to investigate the functional groups and chemical bonds present in the synthesized nanomaterials at the range of 400–4000 cm^{-1} using a FTIR 8400S spectrometer manufactured by Shimadzu corporation, Japan. Transmission electron micrographs (TEM) and selective area electron diffraction (SAED) pattern were acquired to investigate the surface micro-morphological and crystalline information of the sample employing a Talos F200X G2 transmission electron microscope (Thermo Fisher Scientific Company). The acquired TEM images were analyzed by the ImageJ viewer software. The optical properties, in particular the diffusive reflectance spectroscopy (DRS) absorbance and optical band gap of the prepared photocatalysts was studied by a UV–Visible spectrophotometer (UV-2600 Shimadzu, Japan).

Adsorption and photocatalytic experiment

The adsorption and photocatalytic activity of the prepared ZnO and GO-ZnO catalysts were examined against a very well-known and frequently used industrial waste rhodamine B (RhB) dye. In order to study this degradation, at first, a 1000 mL solution of RhB dye with 10 ppm concentration was prepared by mixing it with DI water from which a certain amount of RhB solution was taken in a beaker for each batch experiment. After that, different amount (20, 30 and 50 mg) of our prepared catalysts was added to it and ultrasonicated for few minutes, followed by slow magnetic stirring for next 10 min at dark condition (in the absence of any light) and finally obtained a homogeneous dispersion solution. Then the dispersion solution was left for 60 min at dark condition without any disturbance to achieve the adsorption–desorption equilibrium. Meanwhile, during this adsorption–desorption process, at different time, around 5 mL solution was taken in a spectrophotometer cuvette from the beaker using a micro-filter syringe and absorbance spectra were taken in the wavelength range 400–700 nm using a UV–Visible spectrometer (Model: 1900i, Shimadzu, Japan). From the maximal absorbance value, which is located at 554 nm, the concentration of RhB in the examined solution was determined for each time.

After this, to examine the photocatalytic performance of the photocatalysts, the dispersion solution was irradiated with visible light by a 100 W halogen lamp ($\lambda \geq 400nm$), which provided an average light intensity of ~ 2.9 mW/cm^2. The residual RhB concentration was carried out exactly in the same way as mentioned for adsorption but at different time interval *e.g.* 5, 10, 20, 40 and 60 min. Note that the absorbance of RhB stock solution was measured at the beginning which is termed as RhB blank and considered as the initial concentration of the RhB dye, denoted by C_0.

The recyclability of the superior catalyst GO-ZnO was tested for four consecutive cycles. For this purpose, the GO-ZnO catalyst used in the first cycle was retrieved by centrifugation for 5 min at 8000 rpm, followed by washing with ethanol and DI water for twice to clean the catalyst. Thereafter, to evaporate the residues from the extracted catalyst, it was dried in an air oven for 12 h at 60℃. This recovered nanocatalyst were then reused for next cycles and retrieved exactly in the same way as the first cycle to continue the reusability test. Here we would like to mention that during the recovering process of our GO-ZnO catalysts, a significant amount of catalysts was lost since it involves centrifugation, washing and drying, which hindered us to continue the reusability test after four consecutive cycles.

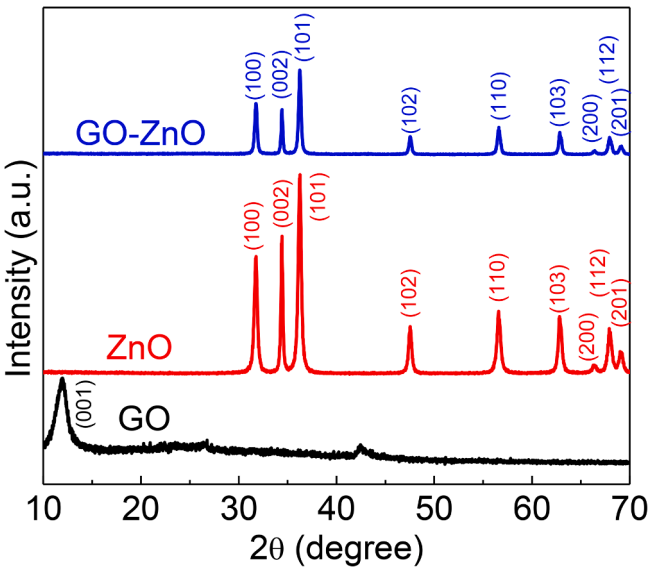

Fig. 1. X-ray diffraction patterns of prepared ZnO NPs and GO-ZnO nanocomposites.

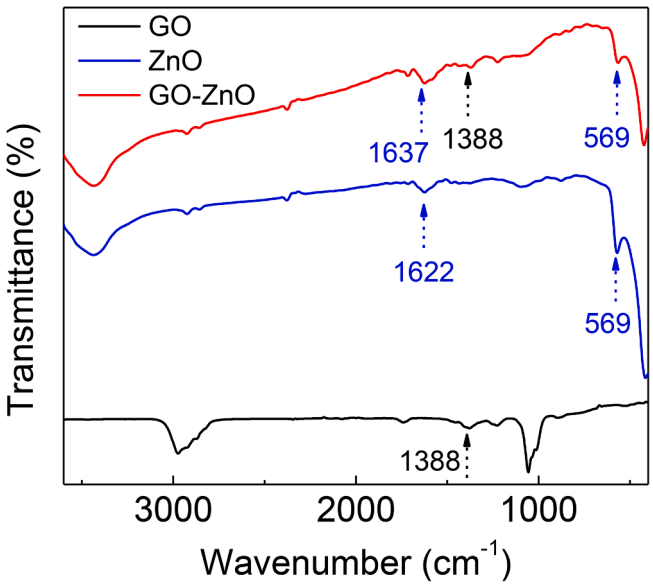

Fig. 2. FTIR spectra of prepared GO, ZnO NPs and GO-ZnO nanocomposites.

Results and discussion

Structural analysis by x-ray diffraction

In the powder x-ray diffraction (PXRD) pattern of graphene oxide (GO) (Fig. 1), the most obvious diffraction peak at $2\theta = 10.67^{\circ}$ is observed, which is the characteristic (001) crystal plane of GO. This PXRD data was employed to determine the $d-$ spacing value and is found as 8.29 Å for the prepared GO sample. This value exactly matched with the reported value and differs from the reported interplanar spacing (3.34 Å) of graphite flakes [54,55] which implies that oxygen functionalities carrying GO is successfully synthesized [56].

PXRD patterns of ZnO and GO-ZnO are presented in Fig. 1. PXRD peaks for ZnO NPs are observed at 2θ = 31.72, 34.37, 36.24, 47.49, 56.52, 62.83, 66.34, 67.92, 69.10 corresponding to (100), (002), (101), (102), (110), (103), (200), (112) and (201) crystal planes respectively. These 2 θ values and the corresponding planes prove that pure ZnO NPs exhibits hexagonal wurtzite closed packing lattice structure (JCPDS: 79-0208) [57,58]. In the PXRD pattern, we noticed that the peaks are very sharp, which illustrates the high crystallinity of the synthesized ZnO NPs sample. When this ZnO NPs are immobilized on GO to form GO-ZnO composites, then no additional peaks were observed, which suggests that no impurity is introduced or remained in the GO-ZnO nanocomposites due to this facile synthesis process. Furthermore, no peaks for pristine GO has been observed in the powder XRD of the prepared composite material. This suggests that GO nanoleaves are thoroughly exfoliated and well dispersed in ZnO NPs by such incorporation and didn't change the wurtzite crystal structure of ZnO nanoparticles. We believe that this happened due to the smaller percentage of GO incorporation and the decreased in regularity in layer attacking of GO sheets due to the intercalation of ZnO nanoparticles. Such diffraction pattern was reported by others when different nanoparticles were immobilized on GO nanosheets [52,53,59,60]. Furthermore, a reduction of intensity can be easily observed in GO-ZnO composite sample, which also reveals the complete dispersion of GO nanoleaves into the composite materials and undoubtedly the presence of chemical interaction between GO and ZnO in GO-ZnO composites [61].

The average crystallite size was calculated using the famous Debye-Scherrer's formula [62]:

$$D = 0.89 \times \frac{\lambda}{\beta cos\theta}$$

Here, $\lambda = 0.154060$ nm is the wavelength of x-ray; β = full width at half maxima; θ=Bragg's diffraction angle for the (101) plane as taken from the highest intensity peak for both ZnO and GO-ZnO samples. The determined crystallite size was found as 23.23 nm and 30.77 nm for unmodified ZnO NPs and GO-ZnO nanocomposites, respectively.

Fourier transform infrared spectroscopy analysis

Fourier transform infra-red (FTIR) spectra of GO, ZnO NPs and GO-ZnO composites were taken in the range from 400 to 3600 cm^{-1} to examine the presence of aspired species and functional groups in these samples and are displayed in Fig. 2. GO exhibits different peaks in the FTIR spectrum, located at 1048 cm^{-1} (C-O bond stretching vibrations), 1388 cm^{-1} (C-H bending vibrations) and 1734 cm^{-1} (C = O carbonyl

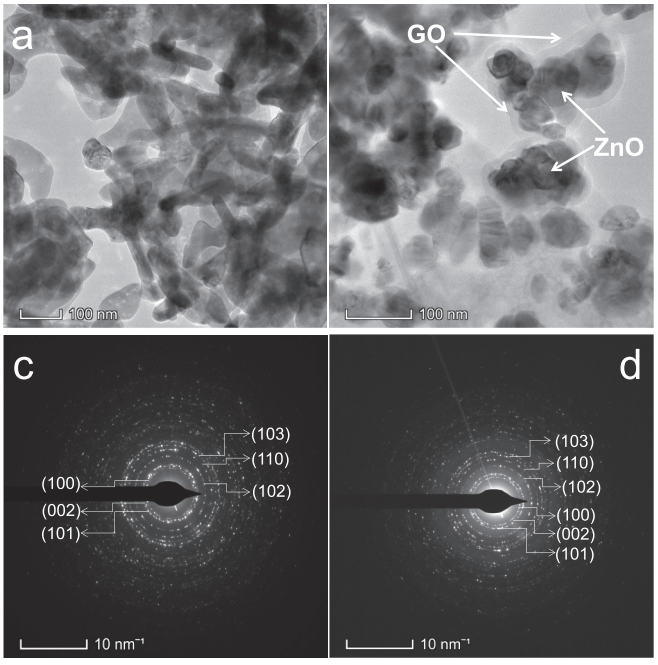

Fig. 3. TEM images of (a) ZnO NPs; (b) GO-ZnO nanocomposites. SAED patterns of (c) ZnO NPs and (d) GO-ZnO nanocomposites.

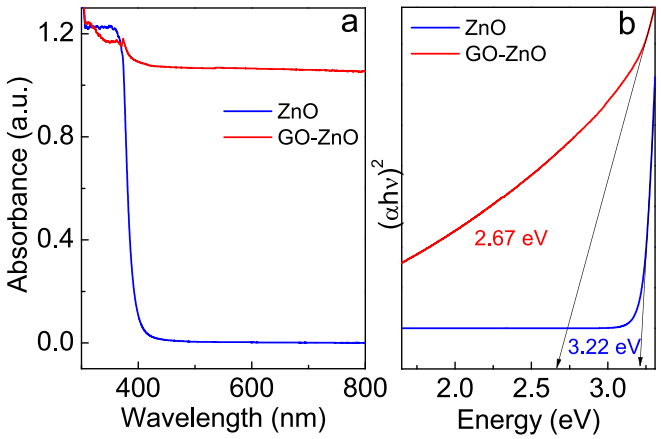

Fig. 4. (a) DRS absorbance and (b) Tauc's plots for ZnO NPs and GO-ZnO nanocomposites.

stretching vibrations). These identified peaks are the most obvious characteristics vibrational bands for GO, which implies the successful synthesis of GO sample. Looking at the FTIR spectrum of ZnO, the most obvious band at 569 cm^{-1} is easily noticeable, which mainly signifies the characteristic Zn-O stretching mode of vibrations [58]. Peak witnessed at 1622 cm^{-1} results from the symmetric and asymmetric vibrations of C═O band for the atmospheric experimental conditions. In the IR spectrum of GO-ZnO composite sample, the C-H bending vibrations for GO has been observed at 1388 cm^{-1}. Also, a shift in wavelength of the C═O band has been observed (from 1622 cm^{-1} to 1637 cm^{-1}) in case of GO-ZnO composite. This confirms the complete exfoliation and dispersion of GO sheets by ZnO NPs. Similar trend has been reported by other in case of nitrogen incorporated ZnO NPs supported on GO nanosheets [61]. Furthermore, the characteristic stretching mode of vibrations for Zn-O was identified at 569 cm^{-1} with a reduction of peak intensity, which happens due to the GO and ZnO hybridization [63]. From these acquired FTIR results, it can be concluded that GO and ZnO NPs are successfully synthesized and thereafter in the GO-ZnO nanocomposite sample, ZnO NPs were immobilized on GO nanosheets, possessing many oxygen containing functional groups.

Study of surface micro-morphology

The surface micro-morphology of the prepared catalysts was assessed by transmission electron microscope and can be viewed in Fig. 3a-b. In the TEM micrographs of ZnO NPs, we noticed that the nanoparticles are quite agglomerated (Fig. 3a). However, in the GO-ZnO composites, it is evident that this particle agglomeration is significantly reduced, which is expected to be beneficial for photocatalytic performance. Also, some wrinkles of GO are easily noticeable at the edge of the composite and ZnO NPs are immobilized onto it. The presence of this GO wrinkle might promote the adsorption of pollutants. Using the acquired TEM image, the average grain size of the samples is determined and found as 25.48 nm and 31.94 nm for ZnO NPs and GO-ZnO composite, respectively. These determined grain sizes are close to the average particle sizes evaluated from PXRD data. Additional to this TEM study, selected area electron diffraction (SAED) measurement was performed and the patterns for ZnO NPs and GO-ZnO composite are shown in Fig. 3c and Fig. 3d, respectively. The SAED patterns demonstrate the Debye-Scherrer rings for the crystal planes (100), (002), (101), (102), (110) and (103), which imply the polycrystalline wurtzite crystal structure of the prepared ZnO nanoparticles and these ZnO NPs are randomly distributed. Interplanar spacing of the crystal planes was evaluated from these SAED patterns by using the ImageJ viewer software and found as 0.229 nm and 0.231 nm, respectively for ZnO NPs and GO-ZnO nanocomposites. These values are close to the previously reported values for wurtzite ZnO NPs [58].

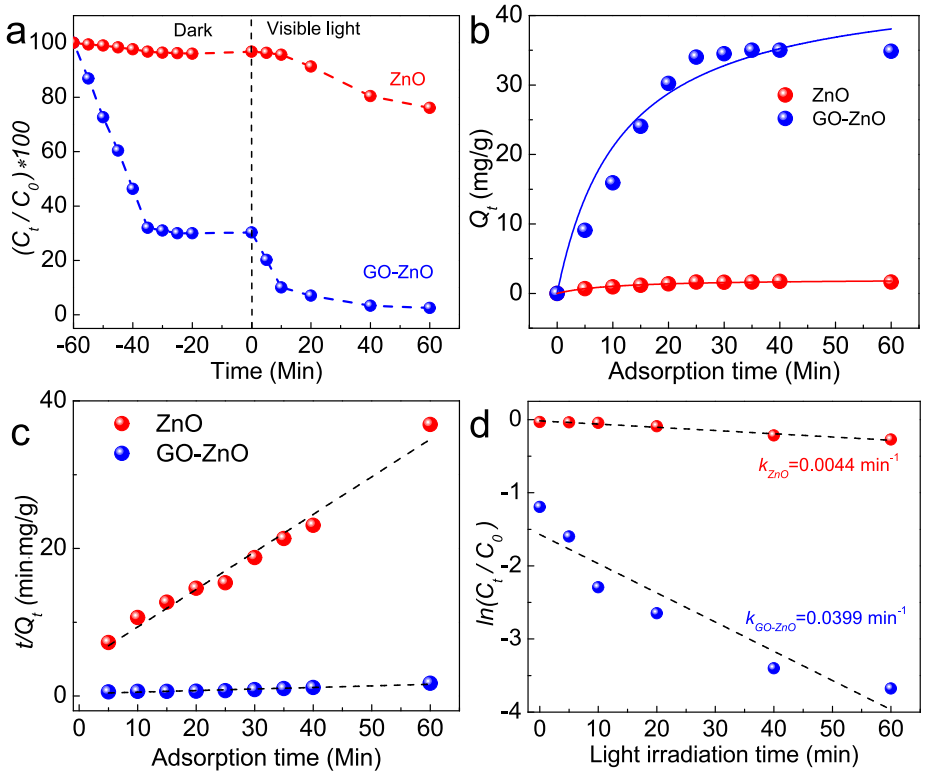

Fig. 5. (a) C_t/C_0 vs *time* plot for adsorption and visible light driven photocatalysis; (b) RhB adsorption capacity of the catalysts over adsorption time; The solid lines represent the pseudo second order kinetic model; (c) Second order kinetic plots for RhB adsorption and (d) apparent first order kinetic curves for visible light irradiated photocatalytic degradation of RhB.

Study of optical properties

UV–visible diffusive reflectance spectroscopy (DRS) was used to study the optical characteristics of the prepared photocatalysts and the absorbance vs wavelength plot is depicted in Fig. 4a. In case of ZnO NPs, we do not see any absorbance of light in the visible wavelength region. On the other hand, GO supported ZnO NPs exhibits very strong visible light absorbance. Incorporation of GO introduces active sites in the composite that results in high affinity to the absorption of visible light. Moreover, the absorption coefficient of graphene oxide is high and it possesses higher surface electric charge under light irradiation [64,65], which all together boost up the visible light absorption by GO-ZnO nanocomposite sample. Therefore, it can be expected that ZnO NPs immobilized on GO nanosheets might be a better visible light driven photocatalyst. To empower this conclusion, the optical band gap of the photocatalysts was calculated using the acquired DRS data by plotting $(\alpha$ h $\nu)^2$ vs h ν and employing Tauc's equation [66]:

$$(\alpha h\nu)^2 = K\left(h\nu - E_g\right).$$

Here "α" is the absorption coefficient, "$h\nu$" is the incident photon energy, "K" is an energy independent constant taken as 1 here. "E_g" is the band gap energy, and the exponent "2" on $\alpha h\nu$ signifies the direct allowed transition. To determine the band gap, a straight line is drawn at the linear part of the $(\alpha$ h $\nu)^2$ vs h ν plot and the $x-$ intercept of this straight line was taken as the optical band gap of the studied photocatalysts (Fig. 4b). The band gap of ZnO NPs is found as 3.22 eV, which is in the UV region. On the other hand, the GO-ZnO nanocomposites possess a reduced band gap of 2.67 eV, which lies within the visible wavelength. This narrowing in band gap along with strong visible light absorption is due to the electrostatic and ionic interactions between graphene oxide and ZnO [67,68].

Adsorption and photoactivity performance

Adsorption and photocatalytic activity of ZnO and GO-ZnO catalysts

The degradation efficiency of both ZnO and GO-ZnO catalysts were examined against RhB dye at dark and under visible light irradiation for different time interval as described in Section 2.4 and are displayed in Fig. S1 and Fig. S2. These absorbance spectra were then used to plot C_t/C_0 vs time (Fig. 5a) and the degradation efficiency which was calculated by the following equation:

degradation efficiency (%) $= \frac{C_0 - C_t}{C_0} \times 100\%$, where C_0 is the initial concentration of RhB dye and C_t is the concentration of the degraded RhB dye at any time t.

In Fig. 5a, it can be seen that the dark adsorption of RhB molecules on to the surface of ZnO NPs is very poor (3.26 %). On the other hand, the composite catalyst exhibits noteworthy adsorption (69.7 %) on its surface at dark condition and this remarkable adsorption happens within a very short contact time (25 min) of GO-ZnO and RhB molecules. Even though the dispersion solution was left in dark condition for 60 min to reach the adsorption–desorption equilibrium conditions and the degradation due to adsorption was recorded for this longer contact time (60 min), the adsorption equilibrium was reached within first 25 min. In the next 35 min of contact time, we do not observe any changes in adsorption since the repulsive forces started to act between adsorbed molecules and existed molecules.

From the visible light driven photocatalytic activity measurements, we see that the photocatalytic degradation of RhB by ZnO photocatalyst is 20 %, which is due to the photosensitization characteristic of RhB. In contrast, better photocatalytic performance (28 %) is achieved when GO-ZnO nanocomposite was used as the photocatalyst. As a whole, it is evident from these studies that GO-ZnO nanocatalyst can outperform unmodified ZnO catalyst in degrading RhB dye due to the combination of 25 min adsorption and 60 min visible light assisted photocatalysis. Since the degradation efficiency of organic pollutants largely depends on adsorbability of pollutants on catalyst surface and the charge transfer capability of the photocatalysts, we analyze the adsorbability and photocatalysis separately in the following paragraphs:

Table 1
Kinetic data of the adsorption and photocatalysis processes.

Sample	Pseudo 2nd order model for adsorption			Pseudo 1st order model for photocatalysis
	Q_e (mg/g)	K_2 (min • g/mg)	R^2 from fit	K (min^{-1})
ZnO	1.97	0.0609	0.9761	0.0044
GO-ZnO	47.62	0.0014	0.9237	0.0399

In order to examine the adsorbability, we calculated the RhB dye uptake Q_t (mg/g) by the catalysts at dark condition using the formula: $Q_t = \frac{[(C_0 - C_t)\times 100 \times V_0 \times M_W]}{W_{\text{catalyst}}}$, where C_0 and C_t are the initial concentration and concentration at time t of RhB dye measured in the time span −60 min to 0 min at dark condition; V_0, M_W and W_{catalyst} are the volume of the solution, molecular weight and the mass of catalyst, respectively [69]. These calculated data was then used to plot Q_t*vs* adsorption time at dark condition (Fig. 5b) and t/Q_t*vs* adsorption time at dark condition (Fig. 5c). Thereafter, the 2nd order model $\frac{t}{Q_t} = \frac{1}{k_2 Q_e^2} + \frac{t}{Q_e}$ was employed to examine the adsorption of RhB molecules on the catalysts surface, the fittings of that model are shown in Fig. 5b (solid lines) and Fig. 5c (dash lines) and the results obtained from these fittings are presented in Table 1. Here, Q_e and Q_t are the amount of adsorption at equilibrium and at time t respectively, and K_2 is the second order kinetic constant, the value of which is obtained from the fitting as 0.0609 min • g/mg and 0.0014 min • g/mg for ZnO NPs and GO-ZnO nanocomposites, respectively (Table 1). From the analyzed results, it is acquired that the adsorption capacity reached 47.62 mg/g in case of GO-ZnO catalyst and this adsorptivity of dye molecules is ∼ 43 times faster in GO-ZnO catalyst with compared to unmodified ZnO NPs. We attribute it to the presence of large 2D planar structure of GO in the composite catalyst with abundant of delocalized π electrons. In detail, GO is electrically negative due to the presence of oxygen based functional groups such as epoxy, hydroxyl, carboxyl [70], whereas RhB is cationic at neutral pH condition [71]. Furthermore, GO possesses larger surface area (∼2600 m^2/g) [72]. As a result, GO based composite (GO-ZnO) interacts with cationic dye RhB via abundant π-π stacking interactions at this neutral pH condition and assist adsorption of RhB molecules onto its larger surface. Another factor for the greater adsorption capacity is the existence of carboxyl, hydroxyl groups in the composite which interact with the –OH groups of dye molecules through hydrogen bonds. All these factors result in greater and faster adsorption capacity of GO-ZnO composite material than pure ZnO NPs.

The photocatalytic activity was studied after the dark adsorption when the solution was irradiated under visible light. In order to do that analysis, the adsorption equilibrium concentration of RhB dye at dark condition was taken as initial concentration (C_o) of RhB for photocatalysis and the concentration of dye at any light irradiation time t is taken as C_t. These data values were then used to plot $ln\left(\frac{C_t}{C_o}\right)$*vs* light irradiation time (t) as can be seen in Fig. 5d. Thereafter, we examined the photocatalytic degradation kinetic of RhB dye by the following apparent-first-order model (dash lines in Fig. 5d) and found that the acquired photocatalytic degradation of studied RhB dye by the prepared photocatalysts follow this 1st order kinetic model [73]: $\ln\left(\frac{C_t}{C_o}\right) = -kt$, where k implies the pseudo first order kinetic rate constant of the photocatalytic reaction. This photocatalytic degradation kinetics has been illustrated in Fig. 5d and from the linear fitted slope of the curves (dash lines in Fig. 5d), the kinetic rate constant (k) was found as 0.0044 min^{-1} and 0.0399 min^{-1} for ZnO and GO-ZnO photocatalysts, respectively. This implies that the photocatalytic degradation is ∼ 9 times rapid when

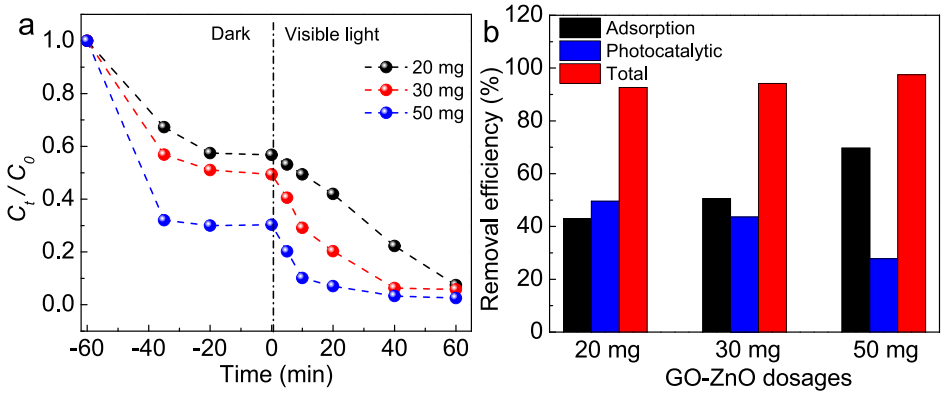

Fig. 6. (a) C_t/C_0 vs *time* plot for three different dosages of GO-ZnO catalyst and (b) effect of GO-ZnO dosages on adsorption, photocatalytic degradation and total removal of RhB dye.

GO-ZnO nanocomposite is irradiated under visible light, whereas this photocatalytic activity is very slow when unmodified ZnO NPs acted as the photocatalyst. The reason of such ultra-fast and enhanced degradation of RhB in case of GO-ZnO photocatalyst can be attributed as follows: The energy band gap (2.67 eV) of GO-ZnO composite falls in visible light wavelength region. As a result, under visible light irradiation, rate of creation of electron hole pair is effective in case of ZnO NPs immobilized on GO (GO-ZnO) photocatalyst. Moreover, addition of zero band gap GO increased the degradation efficiency of GO-ZnO composites because GO can effectively contribute to the adsorption of dye molecules on composite's surface and increase the formation of π-π interaction between the photocatalyst and dye molecules. Furthermore, GO act as photogenerated electrons acceptor from the CB of ZnO, which is then transferred to the surface of the photocatalysts and hinder the electron-hole recombination rate, which all together boost up the ultra-fast photocatalytic degradation efficiency.

Effect of GO-ZnO dosages

To study the effect of GO-ZnO catalyst dosage against RhB dye, the degradation study was carried out for three different dosages (50 mg, 30 mg and 20 mg) and is presented in Figs. S2, S3 and S4, respectively. With the help of these acquired data, the comparative C_t/C_0 vs time and removal efficiency are plotted (Fig. 6a and 6b). It is evident from these figures that with the increase in catalyst dosages, the adsorption capacity of the catalyst increases and becomes maximum for 50 mg GO-ZnO dosage. These results can be explained by the following way: Increasing GO-ZnO dosages implies increased surface area of the catalyst which possesses more oxygen containing functional groups and offers more active sites for the dye molecules to be adsorbed on its surface via π-π interaction between the aromatic ring and GO-ZnO nanocomposite and thereby increase in RhB degradation by adsorption. Meanwhile, the increase of this catalyst dosage slightly reduces the photocatalytic performance, which can be explained from two aspects. Firstly, at higher catalyst dosage, the turbidity of the suspension solution increases which make light dispersed while travelling through the aqueous solution and thereby reduced the influence of light for photocatalysis in the solution [74]. Secondly, when the amount of catalyst is higher, then particle–particle agglomeration, sedimentation and precipitation took place, resulting in reduced active sites for light absorption and as a consequence, the photocatalytic degradation rate decreased [75]. However, the overall RhB removal efficiency is enhanced and the highest value is achieved as 97.7 % for 50 mg GO-ZnO dosage and this ultra-fast removal of RhB occurs within 25 min of adsorption and 60 min of visible light driven photocatalysis process.

The species and role of active radicals during photocatalytic RhB degradation

Organic contaminants are mostly decomposed by reactive species during the photocatalytic process. To find out which reactive species is mainly responsible for the photocatalytic degradation of RhB by GO-ZnO photocatalyst, we carried out the photocatalytic degradation experiment with the help of different scavengers such as ammonium oxalate (AO), tertbutyl alcohol (TBA), 1,4-benzoquinone (BQ) and compared it with the results obtained in the absence of any scavengers under the same experimental conditions. The obtained results are presented in Fig. 7 and found that the removal efficiency decreases in various levels in the presence of different scavengers, confirming the role of diverse reactive species for the RhB dye photo-degradation process. For instance, in the presence of positive hole (h^+) scavenger AO, the photocatalytic degradation efficiency drops only ~6 %, indicating the unobtrusive role of h^+ in RhB dye degradation. When TBA is added to the solution, the photocatalytic degradation efficiency drops ~44 % showing a moderate role of the •OH radical in the process of photo-degradation. Meanwhile, the results show that BQ has a dampening effectiveness of ~78 %, indicating that this scavenger has the greatest inhibitory effect on RhB dye breakdown through photocatalysis. These findings indicate that superoxide radical ($\bullet O_2^-$) is the dominating species in the photocatalytic degradation process of RhB when GO-ZnO acts as visible light driven photocatalyst.

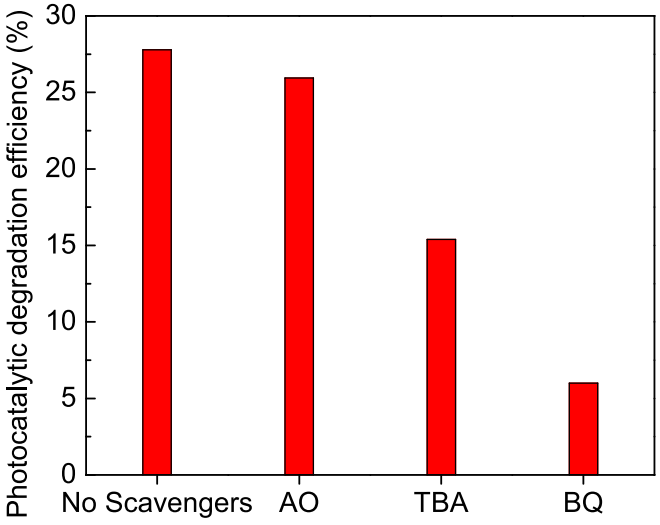

Fig. 7. Role of active species on the photocatalytic degradation of RhB dye using GO-ZnO photocatalyst under visible light irradiation.

Possible degradation mechanism

The degradation of organic effluents depends largely on the adsorption capacity of the catalyst, optical properties, band structure,

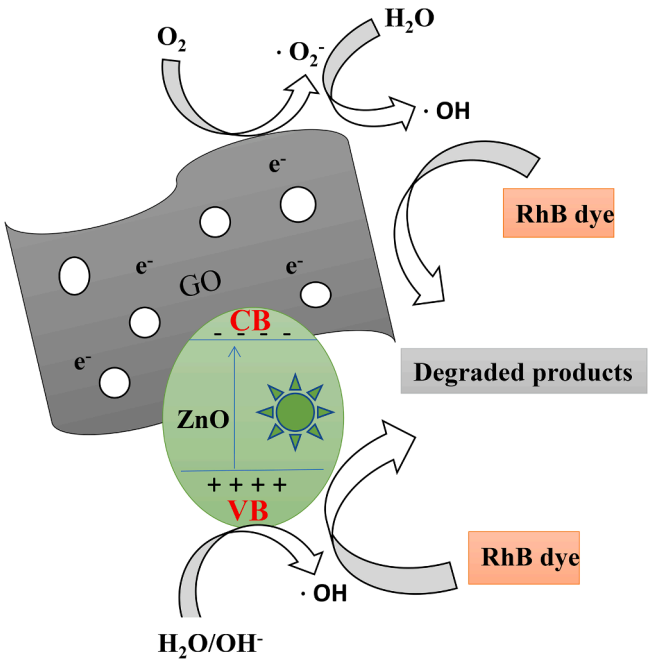

Fig. 8. Degradation mechanism of RhB dye using GO-ZnO nanocatalyst.

etc. [76]. From the aforementioned studies, we propose a degradation mechanism as illustrated in Fig. 8. Under dark condition, RhB dye molecules are adsorb by GO-ZnO catalyst via the electrostatic interaction due to the opposite charge of GO-ZnO catalyst (anionic) and RhB (cationic). When this is irradiated by visible light, then the photo generated electrons transfer to the highly conducting GO nanosheet and inhibit the e-h recombination. These electrons then generate superoxide radicals ($\bullet O_2^-$) by interacting with the surface oxygen molecules. In the meantime, the photo generated holes in the valance band produce hydroxyl (• OH) radicals by interacting with adsorbed water molecule. These superoxide ($\bullet O_2^-$) and hydroxyl (• OH) radicals then react with RhB molecules and disintegrate into smaller non-toxic minerals such as CO_2 and H_2O.

The recovery and reusability of the catalyst

To examine the viability of using GO-ZnO catalyst in practical application, the reusability study was carried out and displayed in Fig. 9a. It is seen that even after back-to-back 4 cycles, our catalyst's degradation efficiency was recorded to be 91.21 % in its 4th cycle against the same initial conditions. A small reduction in degradation efficiency (6 %) may correspond to the loss of sample during the back and forth cycling processes. The PXRD pattern of the recovered GO-ZnO catalyst after 4th cycle demonstrates that the nanocomposite retains its crystal structure as the as prepared GO-ZnO sample but with a small reduction of crystallinity (Fig. 9b). Therefore, it can be inferred that GO-ZnO can be a potential catalyst for wastewater treatment.

A comparative analysis of RhB dye degradation by others

A comparative table regarding RhB dye degradation by different catalysts reported by recent researchers has been shown in Table 2. The parameters and experimental conditions in our studies were comparable with the reported work [29,77–83]. Considering the feasibilities such as source of light for photocatalytic degradation, adsorption and irradiation time, and reusability, it is quite reasonable to use this GO-ZnO catalyst for RhB dye removal from wastewater in a cost-effective and environmental friendly method.

Conclusions

Pristine ZnO NPs and those ZnO NPs immobilized on GO nanosheets were prepared by straightforward and inexpensive ways and their catalytic degradation efficiency was investigated on frequently used rhodamine B (RhB) dye degradation. The GO-ZnO nanocomposite exhibits remarkable adsorption capacity (47.62 mg/g) with the lowest second order kinetic rate constant 0.0014 min • g/mg and visible light driven photocatalytic performance with the apparent first order kinetic rate constant 0.0399 min^{-1}. The GO-ZnO catalyst exhibits the best degradation capability and the degradation efficiency is 97.7 % after 25 min adsorption and 60 min photo-degradation under visible light irradiation, which is 4.2 times higher with compared to unmodified ZnO

Table 2
Comparative data of RhB degradation using different catalysts with this current work.

Catalysts	Time (min)	Degradation (%)	Light Source	Reference
Ce and Bi doped $NiAl_2O_4$	60	90	UV	[77]
Bi_2O_3-ZnO	120	93	Sunlight	[78]
Fe-MOF	90	90	Sunlight	[79]
Fly ash based inorganic polymer	210	94.07	UV	[80]
ZnO/CuO/MoO_3	120	97	Visible	[81]
Z-type BiOCl/Ni-MOF-74 heterojunction	100	97	Visible	[82]
g-C_3N_4-ZnO/Cu_2O	100	91.4	Visible	[83]
Mn and B co-doped mixed phase TiO_2 NPs	90	99	Visible	[29]
GO-ZnO	85	98.7	Visible	Present work

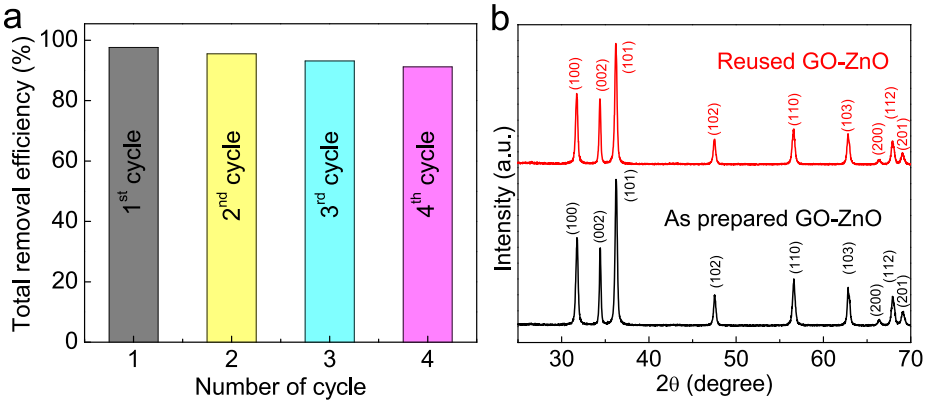

Fig. 9. (a) Demonstration of reusability of GO-ZnO catalyst for the degradation of RhB dye up to four cycles and (b) XRD patterns of the as prepared and reused (four times) GO-ZnO nanocomposite.

catalyst. These excellent catalytic behaviors of GO-ZnO nanocomposite are accredited to the abundant π-π stacking interactions between nanocomposite and dye molecules due to the presence of oxygen functionalities in GO, narrowing of optical band gap for light irradiation, interfacial photogenerated electron transfer from the conduction band of ZnO to the highly conducting GO sheets and lowering of photo-induced electron-hole recombination.

Funding

This research did not receive any specific grant from funding agencies in the public, commercial, or not-for-profit sectors.

CRediT authorship contribution statement

Md. Abdulla Sayem: Writing – original draft, Investigation, Formal analysis, Data curation. **Md Amran Hossen Suvo:** Methodology, Data curation, Formal analysis. **Ishtiaque M. Syed:** Resources, Formal analysis. **Mahabub Alam Bhuiyan:** Conceptualization, Formal analysis, Writing – original draft, Writing – review & editing, Funding acquisition, Project administration, Supervision.

Declaration of competing interest

The authors declare that they have no known competing financial interests or personal relationships that could have appeared to influence the work reported in this paper.

Data availability

Data will be made available on request.

Acknowledgements

We express our gratitude to the Department of Physics, University of Dhaka, Bangladesh. We indebted greatly to the Semiconductor Technology Research Centre (STRC) of the University of Dhaka for giving us the opportunity to use the laboratory facilities rigorously throughout this research. We are grateful to the Centre for Advanced Research in Sciences (CARS) of the University of Dhaka for providing several experimental supports. We would like to acknowledge the Materials Science Division, Bangladesh Atomic Energy Centre, Dhaka, Bangladesh for its TEM support.

Appendix A. Supplementary data

Supplementary data to this article can be found online at https://doi.org/10.1016/j.rinp.2024.107471.

References

[1] Naik SS, Lee SJ, Theerthagiri J, Yu Y, Choi MY. Rapid and highly selective electrochemical sensor based on ZnS/Au-decorated f-multi-walled carbon nanotube nanocomposites produced via pulsed laser technique for detection of toxic nitro compounds. J Hazard Mater 2021;418. https://doi.org/10.1016/j.jhazmat.2021.126269.

[2] Theerthagiri J, et al. Electrocatalytic conversion of nitrate waste into ammonia: a review. Environ Chem Lett 2022. https://doi.org/10.1007/s10311-022-01469-y.

[3] Fida H, Zhang G, Guo S, Naeem A. Heterogeneous Fenton degradation of organic dyes in batch and fixed bed using La-Fe montmorillonite as catalyst. J Colloid Interface Sci 2017;490. https://doi.org/10.1016/j.jcis.2016.11.085.

[4] Lopes OF, Paris EC, Ribeiro C. Synthesis of Nb2O5 nanoparticles through the oxidant peroxide method applied to organic pollutant photodegradation: a mechanistic study. Appl Catal B 2014;144. https://doi.org/10.1016/j.apcatb.2013.08.031.

[5] Yu Y, et al. Method development and mechanistic study on direct pulsed laser irradiation process for highly effective dechlorination of persistent organic pollutants. Environ Pollut Dec. 2021;291:118158. https://doi.org/10.1016/J.ENVPOL.2021.118158.

[6] Mardikar SP, Kulkarni S, Adhyapak PV. Sunlight driven highly efficient degradation of methylene blue by CuO-ZnO nanoflowers. J Environ Chem Eng 2020;8(2). https://doi.org/10.1016/j.jece.2018.11.033.

[7] Theerthagiri J, *et al.*, "Fundamentals and comprehensive insights on pulsed laser synthesis of advanced materials for diverse photo- and electrocatalytic applications," *Light: Science and Applications*, vol. 11, no. 1. Springer Nature, Dec. 01, 2022. doi: 10.1038/s41377-022-00904-7.

[8] Yang S, et al. Enhancement on the removal of Rhodamine B (RhB) by means of the Enlarged Anode Electric Biological (EAEB) reactor. Chemosphere 2020;245. https://doi.org/10.1016/j.chemosphere.2019.125566.

[9] Baldev E, MubarakAli D, Ilavarasi A, Pandiaraj D, Ishack KASS, Thajuddin N. Degradation of synthetic dye, Rhodamine B to environmentally non-toxic products using microalgae. Colloids Surf B Biointerfaces 2013;105. https://doi.org/10.1016/j.colsurfb.2013.01.008.

[10] Ding L, Zhang T, Zhou Y, Liu Q, Zhang L, Li P. Recycled photocatalyst and available photodetector based on ternary $Bi_6Mo_2O_{15}$ sub-microcrystals. Results Phys 2019;13:102117. https://doi.org/10.1016/J.RINP.2019.02.053.

[11] Jenita Rani G, Jothi Rajan MA, Gnana Kumar G. Reduced graphene oxide/$ZnFe_2O_4$ nanocomposite as an efficient catalyst for the photocatalytic degradation of methylene blue dye. Res Chem Intermediates 2017;43(4). https://doi.org/10.1007/s11164-016-2788-0.

[12] Theerthagiri J, et al. Application of advanced materials in sonophotocatalytic processes for the remediation of environmental pollutants. J Hazard Mater Jun. 2021;412. https://doi.org/10.1016/j.jhazmat.2021.125245.

[13] Pang YL, et al. Enhancement of photocatalytic degradation of organic dyes using ZnO decorated on reduced graphene oxide (rGO). Desalination Water Treat 2018;108. https://doi.org/10.5004/dwt.2018.21947.

[14] Cheng M, et al. Hydroxyl radicals based advanced oxidation processes (AOPs) for remediation of soils contaminated with organic compounds: A review. Chem Eng J 2016;284. https://doi.org/10.1016/j.cej.2015.09.001.

[15] Wang P, Zhan S, Xia Y, Ma S, Zhou Q, Li Y. The fundamental role and mechanism of reduced graphene oxide in rGO/Pt-TiO_2 nanocomposite for high-performance photocatalytic water splitting. Appl Catal B 2017;207. https://doi.org/10.1016/j.apcatb.2017.02.031.

[16] Liu B, Chen B, Zhang B. Oily wastewater treatment by Nano-TiO_2-induced photocatalysis: Seeking more efficient and feasible solutions. IEEE Nanotechnol Mag 2017;11(3). https://doi.org/10.1109/MNANO.2017.2708818.

[17] Lee KM, Lai CW, Ngai KS, Juan JC. Recent developments of zinc oxide based photocatalyst in water treatment technology: a review. *Water Res* 2016;88. https://doi.org/10.1016/j.watres.2015.09.045.

[18] Dutta V, et al. An overview on WO_3 based photocatalyst for environmental remediation. J Environ Chem Eng 2021;9(1). https://doi.org/10.1016/j.jece.2020.105018.

[19] Armaković SJ, et al. Photocatalytic activity of the V_2O_5 catalyst toward selected pharmaceuticals and their mixture: influence of the molecular structure on the efficiency of the process. Molecules 2023;28(2). https://doi.org/10.3390/molecules28020655.

[20] Li B, et al. The promising NIR light-driven MO3-x (M = Mo, W) photocatalysts for energy conversion and environmental remediation. Chem Eng J 2022;431. https://doi.org/10.1016/j.cej.2021.134044.

[21] Sun X, Yin S, Luo Q, Wei D, Ma Y, Dai X. CdS/SiI2: a promising two-dimensional materials for photocatalytic water splitting. Results Phys 2022;38. https://doi.org/10.1016/j.rinp.2022.105636.

[22] Kamble GS, et al. BiVO4 as a sustainable and emerging photocatalyst: synthesis methodologies, engineering properties, and its volatile organic compounds degradation efficiency. Nanomaterials 2023;13(9). https://doi.org/10.3390/nano13091528.

[23] Yadav R, Chundawat TS, Surolia PK, Vaya D. Photocatalytic degradation of textile dyes using β-CD-CuO/ZnO nanocomposite. J Phys Chem Solid 2022;165:110691. https://doi.org/10.1016/J.JPCS.2022.110691.

[24] Asthana A, Momeni K, Prasad A, Yap YK, Yassar RS. On the correlation of crystal defects and band gap properties of ZnO nanobelts. Appl Phys A Mater Sci Process 2011;105(4). https://doi.org/10.1007/s00339-011-6554-2.

[25] Di Paola A, García-López E, Marcì G, Palmisano L. A survey of photocatalytic materials for environmental remediation. J Hazard Mater 2012;211–212. https://doi.org/10.1016/j.jhazmat.2011.11.050.

[26] Kumar R, Anandan S, Hembram K, Narasinga Rao T. Efficient ZnO-based visible-light-driven photocatalyst for antibacterial applications. ACS Appl Mater Interfaces 2014;6(15). https://doi.org/10.1021/am502915v.

[27] Anju Chanu L, Joychandra Singh W, Jugeshwar Singh K, Nomita Devi K. Effect of operational parameters on the photocatalytic degradation of Methylene blue dye solution using manganese doped ZnO nanoparticles. Results Phys 2019;12. https://doi.org/10.1016/j.rinp.2018.12.089.

[28] Saeed M, et al. Synthesis of p-n NiO-ZnO heterojunction for photodegradation of crystal violet dye. Alex Eng J 2023;65:561–74. https://doi.org/10.1016/J.AEJ.2022.09.048.

[29] Sultana R, Liba SI, Rahman MA, Yeachin N, Syed IM, Bhuiyan MA. Enhanced photocatalytic activity in RhB dye degradation by Mn and B co-doped mixed phase TiO_2 photocatalyst under visible light irradiation. Surf Interfaces 2023;42. https://doi.org/10.1016/j.surfin.2023.103302.

[30] Azqhandi MHA, Vasheghani BF, Rajabi FH, Keramati M. Synthesis of Cd doped ZnO/CNT nanocomposite by using microwave method: photocatalytic behavior, adsorption and kinetic study. Results Phys 2017;7. https://doi.org/10.1016/j.rinp.2017.02.033.

[31] Verma N, Chundawat TS, Chandra H, Vaya D. An efficient time reductive photocatalytic degradation of carcinogenic dyes by TiO_2-GO nanocomposite. Mater

Res Bull 2023;158:112043. https://doi.org/10.1016/J.MATERRESBULL.2022.112043.
[32] Verma N, Chundawat TS, Surolia PK, Vaya D. Photocatalytic reduction of Cr VI by TiO_2/GO nanocomposite. ChemistrySelect 2022;7(22). https://doi.org/10.1002/slct.202201275.
[33] Pu YC, Chou HY, Kuo WS, Wei KH, Hsu YJ. Interfacial charge carrier dynamics of cuprous oxide-reduced graphene oxide (Cu_2O-rGO) nanoheterostructures and their related visible-light-driven photocatalysis. Appl Catal B 2017;204. https://doi.org/10.1016/j.apcatb.2016.11.012.
[34] Thomas RT, Abdul Rasheed P, Sandhyarani N. Synthesis of nanotitania decorated few-layer graphene for enhanced visible light driven photocatalysis. J Colloid Interface Sci 2014;428. https://doi.org/10.1016/j.jcis.2014.04.054.
[35] Geim AK, Novoselov KS. The rise of graphene. Nat Mater 2007;6(3). https://doi.org/10.1038/nmat1849.
[36] Subramanian V, Wolf EE, Kamat PV. Catalysis with TiO_2/gold nanocomposites. Effect of metal particle size on the Fermi level equilibration. J Am Chem Soc 2004;126(15). https://doi.org/10.1021/ja0315199.
[37] Bhunia SK, Jana NR. Reduced graphene oxide-silver nanoparticle composite as visible light photocatalyst for degradation of colorless endocrine disruptors. ACS Appl Mater Interfaces 2014;6(22). https://doi.org/10.1021/am505677x.
[38] Ong CB, Mohammad AW, Ng LY, Mahmoudi E, Azizkhani S, Hayati Hairom NH. Solar photocatalytic and surface enhancement of ZnO/rGO nanocomposite: Degradation of perfluorooctanoic acid and dye. Process Safety Environ Protect 2017;112. https://doi.org/10.1016/j.psep.2017.04.031.
[39] Gangwar P, Singh S, Khare N. Study of optical properties of graphene oxide and its derivatives using spectroscopic ellipsometry. Appl Phys A Mater Sci Process 2018;124(9). https://doi.org/10.1007/s00339-018-1999-1.
[40] Li YT, Xu JM, Tang ZJ, Xu TT, Li XJ. Nearly white light photoluminescence from ZnO/rGO nanocomposite prepared by a one-step hydrothermal method. J Alloys Compd 2017;715:122–8. https://doi.org/10.1016/J.JALLCOM.2017.04.286.
[41] Kang W, Jimeng X, Xitao W. The effects of ZnO morphology on photocatalytic efficiency of ZnO/RGO nanocomposites. Appl Surf Sci 2016;360:270–5. https://doi.org/10.1016/J.APSUSC.2015.10.190.
[42] Long W, Fu L. Hydrothermal synthesis of ZnO flower-reduced graphene oxide composite for electrochemical determination of ascorbic acid. Fullerenes Nanotubes Carbon Nanostruct 2017;25(7):404–9. https://doi.org/10.1080/1536383X.2017.1324952.
[43] Durmus Z, Kurt BZ, Durmus A. Synthesis and characterization of graphene oxide/zinc oxide (GO/ZnO) nanocomposite and its utilization for photocatalytic degradation of basic fuchsin dye. ChemistrySelect 2019;4(1):271–8. https://doi.org/10.1002/slct.201803635.
[44] Baizaee SM, Arabi M, Bahador AR. A simple, one-pot, low temperature and pressure route for the synthesis of RGO/ZnO nanocomposite and investigating its photocatalytic activity. Mater Sci Semicond Process 2018;82:135–42. https://doi.org/10.1016/J.MSSP.2018.04.004.
[45] Van Tuan P, Phuong TT, Tan VT, Nguyen SX, Khiem TN. In-situ hydrothermal fabrication and photocatalytic behavior of ZnO/reduced graphene oxide nanocomposites with varying graphene oxide concentrations. Mater Sci Semicond Process 2020;115:105114. https://doi.org/10.1016/J.MSSP.2020.105114.
[46] Zhao X, Hu B, Ye J, Jia Q. Preparation, characterization, and application of graphene-zinc oxide composites (G-ZnO) for the adsorption of Cu(II), Pb(II), and Cr (III). J Chem Eng Data 2013;58(9):2395–401. https://doi.org/10.1021/je400384z.
[47] Singh S, et al. Sustainable removal of Cr(VI) using graphene oxide-zinc oxide nanohybrid: Adsorption kinetics, isotherms and thermodynamics. Environ Res 2022;203:111891. https://doi.org/10.1016/J.ENVRES.2021.111891.
[48] Singh S, et al. Multifunctional nanohybrid for simultaneous detection and removal of Arsenic(III) from aqueous solutions. Chemosphere 2022;289:133101. https://doi.org/10.1016/J.CHEMOSPHERE.2021.133101.
[49] Sharma M, et al. Assessment of GO/ZnO nanocomposite for solar-assisted photocatalytic degradation of industrial dye and textile effluent. Environ Sci Pollut Res 2020;27(25):32076–87. https://doi.org/10.1007/s11356-020-08849-3.
[50] Narayanam PK, Botcha VD, Ghosh M, Major SS. Growth and photocatalytic behavior of transparent reduced GO-ZnO nanocomposite sheets. Nanotechnology 2019;30(48). https://doi.org/10.1088/1361-6528/ab3ced.
[51] Sayury Miyashiro C, Hamoudi S. Visible light driven photocatalytic degradation of aqueous acetamiprid over nitrogen and graphene oxide doped ZnO composites. RSC Adv 2021;11(36):22508–16. https://doi.org/10.1039/d1ra02098f.
[52] Peter CN, Anku WW, Sharma R, Joshi GM, Shukla SK, Govender PP. N-doped ZnO/graphene oxide: a photostable photocatalyst for improved mineralization and photodegradation of organic dye under visible light. Ionics (kiel) 2019;25(1):327–39. https://doi.org/10.1007/s11581-018-2571-x.
[53] Wang R, Shi K, Huang D, Zhang J, An S. Synthesis and degradation kinetics of TiO_2/GO composites with highly efficient activity for adsorption and photocatalytic degradation of MB. Sci Rep 2019;9(1). https://doi.org/10.1038/s41598-019-54320-w.
[54] Liu T, Tian L, Graham N, Yang B, Yu W, Sun K. Regulating the interlayer spacing of graphene oxide membranes and enhancing their stability by use of PACl. Environ Sci Technol 2019;53:20. https://doi.org/10.1021/acs.est.9b04418.
[55] Çakmak G, Öztürk T. Continuous synthesis of graphite with tunable interlayer distance. Diam Relat Mater 2019;96. https://doi.org/10.1016/j.diamond.2019.05.002.
[56] Alamelu K, Raja V, Shiamala L, Jaffar Ali BM. Biphasic TiO_2 nanoparticles decorated graphene nanosheets for visible light driven photocatalytic degradation of organic dyes. Appl Surf Sci 2018;430:145–54. https://doi.org/10.1016/J.APSUSC.2017.05.054.
[57] Saravanan R, Gupta VK, Narayanan V, Stephen A. Comparative study on photocatalytic activity of ZnO prepared by different methods. J Mol Liq 2013;181. https://doi.org/10.1016/j.molliq.2013.02.023.
[58] Wasly HS, El-Sadek MSA, Henini M. Influence of reaction time and synthesis temperature on the physical properties of ZnO nanoparticles synthesized by the hydrothermal method. Appl Phys A Mater Sci Process 2018;124(1). https://doi.org/10.1007/s00339-017-1482-4.
[59] Gao P, Liu J, Sun DD, Ng W. Graphene oxide–CdS composite with high photocatalytic degradation and disinfection activities under visible light irradiation. J Hazard Mater 2013;250–251:412–20. https://doi.org/10.1016/J.JHAZMAT.2013.02.003.
[60] Yempally S, Cabibihan JJ, Ponnamma D. A facile approach to develop polyvinyl alcohol-based bio-triboelectric nanogenerator containing graphene- doped zinc oxide quantum dots. Energ Technol 2024. https://doi.org/10.1002/ente.202300992.
[61] Peter CN, Anku WW, Sharma R, Joshi GM, Shukla SK, Govender PP. N-doped ZnO/graphene oxide: a photostable photocatalyst for improved mineralization and photodegradation of organic dye under visible light. Ionics (Kiel) 2019;25(1). https://doi.org/10.1007/s11581-018-2571-x.
[62] Ma X, Zhou W, Chen Y. Structure and photocatalytic properties of Mn-doped TiO_2 loaded on wood-based activated carbon fiber composites. Materials 2017;10(6). https://doi.org/10.3390/ma10060631.
[63] Van Tuan P, Phuong TT, Tan VT, Nguyen SX, Khiem TN. In-situ hydrothermal fabrication and photocatalytic behavior of ZnO/reduced graphene oxide nanocomposites with varying graphene oxide concentrations. Mater Sci Semicond Process 2020;115. https://doi.org/10.1016/j.mssp.2020.105114.
[64] Darvishi M, Jamali-Paghaleh F, Jamali-Paghaleh M, Seyed-Yazdi J. Facile synthesis of ZnO/rGO hybrid by microwave irradiation method with improved photoactivity. Surf Interfaces 2017;9. https://doi.org/10.1016/j.surfin.2017.09.008.
[65] Lv R, et al. Facile synthesis of ZnO nanorods grown on graphene sheets and its enhanced photocatalytic efficiency. J Chem Technol Biotechnol 2015;90(3). https://doi.org/10.1002/jctb.4347.
[66] Tran TH, et al. Sr doped $LaMnO_3$ nanoparticles prepared by microwave combustion method: a recyclable visible light photocatalyst. Results Phys 2020;19. https://doi.org/10.1016/j.rinp.2020.103417.
[67] Mandal SK, et al. Engineering of ZnO/rGO nanocomposite photocatalyst towards rapid degradation of toxic dyes. Mater Chem Phys 2019;223. https://doi.org/10.1016/j.matchemphys.2018.11.002.
[68] Kalantari Bolaghi Z, Masoudpanah SM, Hasheminiasari M. Photocatalytic activity of ZnO/RGO composite synthesized by one-pot solution combustion method. Mater Res Bull 2019;115. https://doi.org/10.1016/j.materresbull.2019.03.024.
[69] Shawabkeh RA, Tutunji MF. Experimental study and modeling of basic dye sorption by diatomaceous clay. Appl Clay Sci 2003;24(1–2):111–20. https://doi.org/10.1016/S0169-1317(03)00154-6.
[70] Li MJ, Liu CM, Bin Cao H, Zhang Y. Surface charge research of graphene oxide, chemically reduced graphene oxide and thermally exfoliated graphene oxide. Adv Mat Res 2013. https://doi.org/10.4028/www.scientific.net/AMR.716.127.
[71] Kaur H, Kaur R. Removal of Rhodamine-B dye from aqueous solution onto Pigeon Dropping: adsorption, kinetic, equilibrium and thermodynamic studies. J Mater Environ Sci 2014;5(6).
[72] Wang X, Wang C, Dai S. Chalcogenide glass-tapered fiber sensor modified by graphene oxide doped with platinum nanoparticles for high-sensitivity measurement. Results Phys 2023;47. https://doi.org/10.1016/j.rinp.2023.106348.
[73] Al-Rawashdeh NAF, Allabadi O, Aljarrah MT. Photocatalytic activity of graphene oxide/zinc oxide nanocomposites with embedded metal nanoparticles for the degradation of organic dyes. ACS Omega 2020;5(43). https://doi.org/10.1021/acsomega.0c03608.
[74] Ahmed S, Rasul MG, Brown R, Hashib MA. Influence of parameters on the heterogeneous photocatalytic degradation of pesticides and phenolic contaminants in wastewater: A short review. J Environ Manage 2011;92(3):311–30. https://doi.org/10.1016/J.JENVMAN.2010.08.028.
[75] Safari GH, Hoseini M, Seyedsalehi M, Kamani H, Jaafari J, Mahvi AH. Photocatalytic degradation of tetracycline using nanosized titanium dioxide in aqueous solution. Int J Environ Sci Technol 2015;12(2):603–16. https://doi.org/10.1007/s13762-014-0706-9.
[76] Asif M, Saeed M, Zafar M, Amjad UeS, Razzaq A, Young Kim W. Development of Co-Al LDH/GO composite photocatalyst for enhanced degradation of textile pollutant under visible light irradiation. Results Phys 2022;42. https://doi.org/10.1016/j.rinp.2022.105997.
[77] Chellammal Gayathri R, Elakkiya V, Sumathi S. Synthesis of cerium and bismuth doped nickel aluminate for the photodegradation of methylene blue, methyl orange and rhodamine B dyes. Chemosphere 2022;303. https://doi.org/10.1016/j.chemosphere.2022.135056.
[78] Yasin M, et al. Development of Bi_2O_3-ZnO heterostructure for enhanced photodegradation of rhodamine B and reactive yellow dyes. Surf Interfaces 2022;30. https://doi.org/10.1016/j.surfin.2022.101846.
[79] Pattappan D, Vargheese S, Kavya KV, Kumar RTR, Haldorai Y. Metal-organic frameworks with different oxidation states of metal nodes and aminoterephthalic acid ligand for degradation of Rhodamine B under solar light. Chemosphere 2022;286. https://doi.org/10.1016/j.chemosphere.2021.131726.
[80] El Alouani M, et al. Synergetic influence between adsorption and photodegradation of Rhodamine B using synthesized fly ash based inorganic polymer. Surf Interfaces 2021;24:101136. https://doi.org/10.1016/J.SURFIN.2021.101136.
[81] Hussain MK, Khalid NR, Tahir MB, Tanveer M, Iqbal T, Liaqat M. Enhanced visible light-driven photocatalytic activity and stability of novel ternary ZnO/CuO/MoO_3

nanorods for the degradation of rhodamine B and alizarin yellow. Mater Sci Semicond Process 2023;155. https://doi.org/10.1016/j.mssp.2022.107261.

[82] Xu M, et al. A novel Z-type BiOCl/Ni-MOF-74 heterojunction with coral reef-like structure for photodegradation of tetracycline and rhodamine B and degradation pathway analysis. Mater Sci Semicond Process 2023;168. https://doi.org/10.1016/j.mssp.2023.107832.

[83] Rajendran R, et al. Investigation on novel Cu_2O modified g-C_3N_4/ZnO heterostructures for efficient photocatalytic dye degradation performance under visible-light exposure. Colloids Interface Sci Commun 2021;44. https://doi.org/10.1016/j.colcom.2021.100480.